Research Square

Preprints are preliminary reports that have not undergone peer review.
They should not be considered conclusive, used to inform clinical practice,
or referenced by the media as validated information.

Therapeutic Efficacy of a Novel K62-Specific Phage Depolymerase Against Klebsiella pneumoniae

Can Wang
The Fifth affiliated hospital of Anhui Medical University
Ruilin Yang
The Fifth affiliated hospital of Anhui Medical University
Jinpan Wei
The Fifth affiliated hospital of Anhui Medical University
Lei Zhao
ayefyzhaolei@163.com
The Fifth affiliated hospital of Anhui Medical University

Research Article

Keywords: Antibiotic resistance, Depolymerase, K62, Klebsiella pneumoniae, Lethality, Phage, Phylogenetic analysis, Webervirus

Posted Date: July 1st, 2026

DOI: https://doi.org/10.21203/rs.3.rs-10118169/v1

License: This work is licensed under a Creative Commons Attribution 4.0 International License.
Read Full License

Additional Declarations: No competing interests reported.

Version of Record: A version of this preprint was published at Folia Microbiologica on October 9th, 2026. See the published version at https://doi.org/10.1007/s12223-026-01605-z.

Abstract

Multidrug-resistant *Klebsiella pneumoniae* has emerged as a formidable healthcare challenge, driving the urgent need for alternative therapeutic strategies such as phage therapy. In this study, we isolated and comprehensively characterized a novel phage, designated vB_Kp_IME328 (IME328), which exhibits highly specific bactericidal activity against K62-type *K. pneumoniae*. Morphological analyses revealed that IME328 forms plaques surrounded by distinct translucent halos and possesses a long tail, clustering it within the *Webervirus* genus. Through whole-genome sequencing and bioinformatic analysis, we identified *ORF3* as the gene encoding a putative tail-fiber depolymerase. This gene was successfully cloned and expressed, yielding the recombinant protein Dp3. Functional assays confirmed that Dp3 possesses robust depolymerizing and antibacterial activities. *In vitro*, Dp3 acted synergistically with serum to effectively eradicate the target bacteria. Furthermore, live/dead cell staining and cellular assays demonstrated that Dp3 significantly enhances the phagocytic and intracellular bactericidal capacities of macrophages. *In vivo* evaluations using a lethal murine bacteremia model (inoculated with 6×10^7 CFU) showed that Dp3 administration conferred 100% protection and survival, whereas all untreated infected mice succumbed to the infection. Together, our findings highlight the remarkable, targeted antibacterial efficacy of IME328 and its depolymerase Dp3, offering a highly promising therapeutic candidate for combating severe, antibiotic-resistant *K. pneumoniae* infections.

1. Introduction

Klebsiella pneumoniae is a ubiquitous opportunistic pathogen responsible for a myriad of severe clinical conditions, including urinary tract infections, bacteremia, pneumonia, and liver abscesses (Wang et al. 2020c; Wu et al. 2023a). The rapid global dissemination of carbapenem-resistant *K. pneumoniae* (CRKP) since its initial detection in 1996 has elevated this pathogen to a critical public health threat, severely limiting available treatment options (Ding et al. 2026; Hua et al. 2022). A primary determinant of *K. pneumoniae* virulence is its robust capsular polysaccharide (CPS), also known as the K antigen. This thick outer layer acts as a formidable physical barrier that impairs antibiotic penetration, dampens the efficacy of antimicrobial peptides, and thwarts host immune clearance mechanisms, such as complement-mediated lysis and macrophage phagocytosis(Choi et al. 2020). The structural complexity of the CPS is vast; to date, approximately 80 serologically defined K types and over 140 distinct genetic capsule loci have been identified (Pan et al. 2015). This extensive serotypic diversity dictates variations in virulence and complicates the clinical management of *K. pneumoniae* infections, underscoring the urgent need for nuanced, serotype-specific therapeutic strategies (Cano et al. 2009). In the face of dwindling antibiotic efficacy, bacteriophages (phages) have emerged as a highly promising alternative for combatting refractory infections(Brenes and Laub 2025; Huang et al. 2024a; Monteiro et al. 2019). Phages possess the inherent ability to specifically recognize, infect, and lyse host bacteria, even those shielded by dense polysaccharide capsules. Both *in vitro* and *in vivo* studies have demonstrated the encouraging potential of phage therapy against *K. pneumoniae(*Nang et al. 2024; Yin et al. 2026). A critical weapon in the phage replication arsenal is the polysaccharide depolymerase, an enzyme that specifically degrades the bacterial CPS (Park 1956; Yan et al. 2014). By stripping away this protective

layer, depolymerases expose the bacterial outer membrane, facilitating phage attachment and sensitization of the pathogen to host immunity. Due to their strict structural specificity, these enzymes serve as not only potent, narrow-spectrum antibacterial agents but also cost-effective tools for rapid capsule typing (Pan et al. 2019). While depolymerases targeting 23 different *K. pneumoniae* serotypes - including K1, K2, K7, K20, K27, K47, and K64, the latter two being predominant in China-have been previously characterized (Dunstan et al. 2021; Gorodnichev et al. 2021; Li et al. 2021a; Li et al. 2021b; Pertics et al. 2021; Squeglia et al. 2020; V Volozhantsev et al. 2020; Wu et al. 2023b; Wu et al. 2019), the current repertoire remains insufficient to cover the full spectrum of clinically relevant strains.

To expand the arsenal of targeted treatments against CRKP, this study aimed to isolate and characterize a novel bacteriophage specifically targeting the K62 serotype of *K. pneumoniae*. Here, we detail the discovery of this phage and highlight the practical implications of its derived depolymerase. Our findings demonstrate the dual potential of this newly identified enzyme for both rapid diagnostic application (capsule typing) and therapeutic intervention against K62-type CRKP. The insights gained from this study provide a critical advancement in the development of bespoke, precision antimicrobial strategies to combat highly resistant bacterial strains.

2. Materials and methods

2.1. Isolation and identification of *K. pneumoniae* strains

For this study, we sourced 230 *K. pneumoniae* strains from the State Key Laboratory of Pathogens and Biosecurity at the Beijing Institute of Microbiology and Epidemiology. The 16S rRNA gene was detected as a molecular marker for bacterial identification because of its consistent presence in different bacterial species. Sequencing the 16S rRNA gene facilitated the identification of all *K. pneumoniae* strains. Capsule types of the *K. pneumoniae* strains were determined by sequencing the WZC gene (Pan et al. 2013). Bacterial colonies were counted after growth on Luria Bertani (LB) agar plates (1.5% w/v). All strains were cultured in LB broth (Thermo Scientific, USA) at 37°C and stored in 50% glycerol at -80°C.

2.2. Phage purification and transmission electron microscope (TEM) analysis

The IME328 phage was purified according to Wang's method (Wang et al. 2019) with some modifications. Briefly, a mixture containing 100 µL diluted IME328 and 500 µL logarithmic-phase Kp930 was prepared in 5 mL semi-solid LB medium. This mixture was then evenly spread on a double-layer agar plate and incubated overnight at 37°C. A single phage plaque was carefully selected from the agar plate using a sterilized instrument and introduced into a culture of Kp930 in the logarithmic growth phase (optical density [OD600] = 0.6–0.8) for further incubation. After 3 h incubation, the culture was centrifuged and the supernatant was passed through a 0.22 µm filter to eliminate debris and bacterial cells. These purification steps were repeated thrice to ensure consistent plaque formation, which is crucial for phage isolation and purification.

Next, 35 mL of purified phage supernatant was layered over a sucrose density gradient in a Beckman centrifuge tube. Sequential layers of 20, 25, and 30% (w/v) sucrose solutions were carefully added starting from the bottom of the tube. The tube, duly balanced, was centrifuged at 30000 · *g* at 4°C for 3 h. After centrifugation, the liquid was decanted and the tube was inverted for complete sucrose drainage. Subsequently, 200 µL of 1× TEN buffer was gently added to the bottom of the tube, and the tube was incubated at 4°C overnight. For visualization, 25 µL of the purified IME328 suspension was mixed with an equal volume of 4% paraformaldehyde and 0.5% glutaraldehyde. The resulting mixture was applied to a carbon-coated copper grid for 15 min and stained with 2% phosphotungstic acid for 30 min. The prepared IME328 sample was subsequently examined under a Philips TECNAI-10 transmission electron microscope (TEM) (Holland) (Wang et al. 2020a).

2.3. Phage DNA extraction, genome sequencing, and bioinformatics analysis

Phage DNA extraction, genome sequencing, and bioinformatics analysis of IME328 were conducted using slightly modified versions of our previously established methods(Wang et al. 2020b). The phage suspension was treated overnight at 37°C with 1 mg/mL each of DNase I and RNase A (both from Takara, Dalian, China) to eliminate bacterial nucleic acids, followed by inactivation at 80°C for 15 min. The sample was then mixed with a lysis buffer (comprising 0.5% sodium dodecyl sulfate, 20 mM ethylenediaminetetraacetic acid, and 50 mg/mL protease K), incubated at 56°C for 1 h, and extracted using the standard phenol/chloroform procedure. DNA was precipitated by incubation with an equal volume of isopropanol at -20°C for at least 2 h, followed by centrifugation at 12000 × *g* at 4°C for 10 min. The DNA was washed twice with 75% ethanol, air-dried, and resuspended in nuclease-free water.

Whole-genome sequencing of phage IME328 was performed using a MiSeq system (Illumina, San Diego, CA, USA), and raw data were assembled using Newbler software (version 2.9). The genome sequence of IME328 was annotated online using rapid annotation with subsystem technology (Jaiswal et al. 2023). Open reading frames (ORFs) were identified with the National Center for Biotechnology Information (NCBI) Database using BLASTn and ORF Finder software. ORFs were then verified and classified into different functional proteins using CLC Genomics Workbench software (version 12.0). A comprehensive BLAST search of the IME328 genome was conducted using the NCBI NR Database to identify the most closely related sequences. The IME328 genome and its similarities and differences versus other genes were analyzed using Mauve software (version 2.3.1). The complete genome sequence of IME328 was deposited in GenBank under accession number OK138555.

2.4. Phylogenetic analysis

A phylogenetic tree was constructed for phage IME328 by analyzing the terminase large subunit gene using the adjacency method with 1000 bootstrap replicates (Mohammadi et al. 2023). Evolutionary distances were calculated using Poisson's correction, and the relationships were visualized using MEGA6 software (Brunner et al. 2016). Evolutionary analysis based on tail-protein amino acid sequences

was conducted for phages closely related to IME328, using a method similar to that applied to study evolutionary tree branching for IME328.

2.5. Protein expression and activity validation

The IME328-ORF3 gene was successfully amplified using two specific primers, namely IME328-ORF3-F (5'-CAGCAGATGGACATATACAGAGAAGG-3') and IME328-ORF3-R (3'-CTCGAGTAAACAGGACGTAAGTTCT-5'). The amplified gene fragment was cloned into the p*EASY*^{R}-Blunt E1 expression vector, which contains an efficient promoter for gene expression, using a blunt-ended cloning site for straightforward gene insertion. This vector has an N-terminal 6· His tag, which is typically used for protein purification via metal-affinity chromatography.

Following cloning, the recombinant plasmid was validated by DNA sequencing to ensure accurate incorporation of the target gene sequence. The validated plasmid was transformed into *Escherichia coli* BL21 (DE3) cells. BL21 cells harboring the recombinant plasmid were cultivated at an OD_{600} value of 0.8, indicative of the optimal cell density for protein expression. Recombinant protein expression was then induced with 0.1 mM isopropyl-β-D-thiogalactoside.

After induction, the bacterial culture was centrifuged to separate the cells from the growth medium. The cell pellet was resuspended in lysis buffer containing Tris-HCl, NaCl, glycerol, and phenylmethylsulfonyl fluoride (a protease inhibitor). After lysis and centrifugation, the supernatant (containing soluble proteins) was collected. Protein purification was conducted using an Ni-NTA affinity column (Sangon Biotech, Shanghai, China), taking advantage of the His-tag. The purified protein was eluted in a stepwise manner using an imidazole gradient starting at 20 mM, followed by 40 mM.

2.6. Determination of depolymerase-activity and cleavage spectra of phage IME328

The activity spectrum of the IME328 phage depolymerase and its host range were determined using the double-layer agar plate method. Briefly, IME328 phages and various *K. pneumoniae* strains were incubated at 37°C for 6 h. The plaque-forming units (PFUs) were calculated for each combination of IME328–*K. pneumoniae* strain combination. Clear zones formed on the bacterial lawns due to lytic phage activity were observed. The efficiency of plating (EOP) was calculated by dividing the average number of PFUs for the phage with a target bacterium by the average number of PFUs observed with a reference host bacterium. Determining the EOP enabled quantitative assessments of the phage-replication efficiency in different bacterial strains in a previous study (Khan Mirzaei and Nilsson 2015). Furthermore, the cleavage spectrum of phage IME328 was determined using spot tests for 230 *K. pneumoniae* strains with known capsular types. The presence or absence of plaques in these tests indicated the ability of the phage to infect and replicate in different *K. pneumoniae* strains.

2.7. Serum-sensitivity testing

Serum-sensitivity tests were conducted as previously described (Liu et al. 2020a; Pan et al. 2015), with minor modifications. Briefly, six blood samples from healthy volunteers were collected and centrifuged at 1000 × *g* for 10 min to recover the serum. Kp930 cells were cultured overnight, centrifuged, and resuspended in phosphate-buffered saline. Kp930 resuspended PBS was treated for 30 min with Dp3 (10 μg/mL). Subsequently, the treated Dp3 and bacterial suspensions were mixed. These mixtures were then combined with either active serum or inactivated serum (heated at 56°C for 30 min) at a 1:3 volume ratio in a total volume of 100 μL. The mixtures were incubated at 37°C for 1 h. The control group comprised untreated bacteria incubated with Dp3 or active serum. The reaction mixtures were diluted using multiple ratios to facilitate bacterial counting. The assays were performed in three independent experiments.

2.8. Live/dead bacterial viability assay

To evaluate the synergistic bactericidal effect of the depolymerase Dp3 and serum, a LIVE/DEAD Bacterial Staining Kit with DMAO & PI (Cat. No. C2030, Beyotime Biotechnology, China) was employed according to the manufacturer's protocol. Briefly, bacteria in the logarithmic growth phase were treated with either PBS (Control) or a combination of Dp3 and active serum. Following incubation, the bacterial suspensions were centrifuged at 10,000 × g for 5 min at room temperature. The pellets were washed once with sterile saline and resuspended to an approximate density of 10^8 bacteria/mL. The bacterial suspensions were then mixed with the DMAO/PI staining working solution and incubated in the dark at 37°C for 15 min. DMAO is a membrane-permeable dye that preferentially binds to double-stranded DNA and stains both live and dead bacteria green. PI is membrane-impermeable and only enters cells with compromised membranes, emitting red fluorescence. The stained samples were immediately applied to glass slides and observed using a fluorescence microscope.

2.9. Macrophage phagocytosis and adhesion assay

The murine macrophage cell line RAW264.7 was cultured in DMEM supplemented with 10% fetal bovine serum (FBS) at 37°C with 5% CO2. Cells were seeded into confocal dishes and grown to approximately 90% confluence. Target bacteria in the logarithmic growth phase were harvested, resuspended in PBS to an OD600 of 0.5, and incubated with fluorescein isothiocyanate (FITC; 0.5 mg/mL final concentration) in the dark at 4°C for 1 h. Following the quenching of unreacted FITC with glycine, the labeled bacteria were washed and pre-treated with either Dp3 or PBS (Control). The RAW264.7 macrophages were then co-incubated with the bacterial suspension at a multiplicity of infection (MOI) of 10:1. After the co-incubation period, the cells were washed thoroughly with PBS to remove unbound and non-phagocytosed bacteria. The interaction, including adherence and internalization of the FITC-labeled bacteria by the macrophages, was subsequently observed and recorded using a fluorescence microscope.

2.10. Animal Infection Model and Survival Analysis

To evaluate the *in vivo* protective efficacy of the depolymerase Dp3, mice were randomly divided into experimental groups. The infection model was established by administering a lethal dose of *Klebsiella pneumoniae* (6× 10^7 CFU). The treatment group received Dp3 intervention following infection. The

survival of the mice was continuously monitored for 96 hours, and Kaplan-Meier survival curves were generated to evaluate the impact of Dp3 on the survival rate.

2.11. Determination of Bacterial Load in Organs

Mice from the untreated infection group (when moribund) and the Dp3-treated group were euthanized for bacterial burden analysis. The liver, spleen, lung, and kidney were aseptically harvested, weighed, and homogenized in sterile PBS. The tissue homogenates were serially diluted and plated onto agar plates. After overnight incubation at 37°C, colonies were counted. The bacterial loads were expressed as Log10CFU/g of tissue.

2.12. Histopathological Evaluation

Target organs (liver, spleen, lung, and kidney) from the healthy control group, the bacterial infection group (Kp930), and the Dp3 treatment group were harvested and fixed in 4% paraformaldehyde for at least 24 hours. The tissues were then dehydrated, embedded in paraffin, and sectioned (4–5 μm thickness). Hematoxylin and eosin (H&E) staining was performed, and the slides were observed under a light microscope to evaluate histopathological damage and tissue recovery.

2.13. Statistical analysis

All experimental data are presented as mean ± SD. Independent Student's *t*-test was employed for comparing two groups, and two-way analysis of variance (ANOVA) was utilized for comparing multiple groups. All analyses were conducted and visualized using Prism 6 software (GraphPad Software, CA, USA). A value of $P < 0.05$ was considered statistically significant

3. Results

3.1. *K. pneumoniae* capsule typing

A total of 230 *K. pneumoniae* strains were typed via WZC gene sequencing. Among these, various types were identified, including five K62 strains and several K1, K2, and K3 strains (Table 1). The drug-sensitivity profile of Kp930 is shown in Table 2.

Table 1

List of Kp strains used in wzc and their typing results, including sensitivity to different phages and the depolymerase, Dp3

K type	Bacterial isolates	Sensitivity to phage	Sensitivity to depolymerase
K1	Kp217, Kp229, Kp230, Kp960, Kp995, Kp402, Kp1155, Kp607, Kp2406, Kp2418, Kp2521, Kp2755	-	-
K2	Kp336, Kp1011, Kp1215, Kp1408, Kp1860, Kp38, Kp45, Kp56, Kp72, Kp200, Kp226, Kp551, Kp696, Kp1118, Kp2361, Kp2750, Kp2763	-	-
K3	Kp195, Kp497	-	-
K5	Kp66, Kp120	-	-
K7	Kp272	-	-
K12	Kp55, Kp474, Kp702, Kp787	-	-
K14	Kp24, Kp2391, Kp2051, Kp2575	-	-
K15	Kp938, Kp954, Kp955, Kp1053, Kp1073, Kp1079, Kp1080, Kp1082, Kp1098, Kp1100, Kp1241, Kp1763, Kp1788, Kp1809, Kp2061, Kp2062, Kp2095, Kp2098, Kp180, Kp1744, Kp1751, Kp2358, Kp2498, Kp2061, Kp2613	-	-
K19	Kp231, Kp970, Kp948, Kp1416, Kp2412, Kp2419	-	-
K20	Kp1852, Kp592, Kp899, Kp844	-	-
K24	Kp2897, Kp2914, Kp2435, Kp2058, Kp2063, Kp2674, Kp2483	-	-
K25	Kp439, Kp626, Kp1745, Kp1757	-	-
K28	Kp573, Kp2384, Kp2858, Kp2859, Kp2782, Kp2484, Kp2780, Kp2493	-	-
K39	Kp1000, Kp1301, Kp1307	-	-
K47	Kp3, Kp51, Kp1183, Kp1618, Kp1619, Kp1620, Kp1621, Kp1642, Kp1732, Kp1737, Kp1740, Kp1812, Kp1616, Kp1738, Kp1746, Kp1563, Kp1615, Kp1617, Kp2238, Kp2240, Kp2059, Kp2097, Kp2234, Kp2235, Kp2236, Kp2237, Kp2353, Kp2407, Kp2408, Kp2409, Kp2411, Kp2413, Kp2416, Kp2417, Kp2522	-	-
K54	Kp828, Kp853, Kp1020, Kp2709, Kp2710, Kp2789	-	-
K57	Kp280, Kp369, Kp578, Kp1185, Kp1304, Kp5, Kp1117, Kp1150, Kp1151	-	-
K62	Kp930, Kp1216, Kp1023, Kp1770, Kp2587	+	+

K, *Klebsiella*; -, insensitive; +, sensitive

K type	Bacterial isolates	Sensitivity to phage	Sensitivity to depolymerase
K63	Kp465, Kp501, Kp576, Kp1165, Kp1171, Kp2574	-	-
K64	Kp982, Kp610, Kp2380, Kp2381, Kp2385, Kp2393, Kp2685, Kp2431, Kp2432, Kp2433, Kp2434, Kp2435, Kp2448, Kp2451, Kp2452, Kp2455, Kp2456, Kp2457, Kp2458, Kp2442, Kp2446, Kp2447, Kp2479, Kp2477, Kp2462, Kp2463, Kp2549, Kp2551, Kp2554, Kp2558, Kp2584, Kp2899, Kp2780, Kp2635, Kp2638, Kp2514, Kp2500, Kp2507, Kp2512, Kp2490, Kp2498, Kp2597, Kp2614, Kp2783, Kp2491, Kp2792, Kp2503, Kp2514, Kp2500, Kp2507, Kp2512, Kp2490, Kp2498, Kp2597, Kp261, Kp4, Kp2783, Kp2491, Kp2792, Kp2503, Kp2628, Kp2631, Kp2671	-	-
K81	Kp760, Kp1403, Kp1557, Kp2068	-	-
KN1	Kp409	-	-
KN2	Kp1096, Kp2390	-	-
K, *Klebsiella*; -, insensitive; +, sensitive			

Table 2
Drug-sensitivity data for Kp930

Antibiotic	MIC (μg/ml)	Sensitivity	Antibiotic	MIC (μg/ml)	Sensitivity
Ampicillin	≥ 32	R	Aztreonam	16	R
Ampicillin/sulbactam	≥ 32	R	Imipenem	≤ 1	S
Piperacillin	≥ 128	R	Meropenem	≤ 0.25	S
Piperacillin/tazobactam	16	R	Amikacin	≤ 2	S
Cefazolin	≥ 64	R	Gentamicin	≥ 16	R
Cefuroxime	≥ 64	R	Tobramycin	8	I
Cefuroxime axetil	≥ 64	R	Ciprofloxacin	≥ 4	R
Cefotetan	32	I	Levofloxacin	≥ 8	R
Ceftazidime	16	R	Nitrofurantoin	256	R
Ceftriaxone	≥ 64	R	Cotrimoxazole	160	R
Cefepime	4	I			
Abbreviations: I, insensitive; MIC, minimum inhibitory concentration; R, resistant; S, sensitive					

3.2. Morphological characteristics of bacteriophages

Phage vB_KpnM_IME285, short as IME328, was isolated from an *K. pneumoniae*, named Kp930. Phage IME328 formed transparent plaques on double-layered agar plates (Fig. 1A). Each plaque was surrounded by a semi-transparent halo, indicating that the phage proteins had antibacterial activity. TEM analysis revealed the morphological features of IME328: the icosahedral head measured approximately 50 ± 3 nm in diameter, and the long tail was approximately 150 ± 5 nm long. These characteristics, particularly the icosahedral head and the elongated tail, suggest that IME328 belongs to the *Siphoviridae* family (Fig. 1B).

3.3. Genomic-sequence analysis and alignments for phage IME328

Phage IME328 possesses a double-stranded linear DNA genome, totaling 48,841 base pairs in length (GenBank accession number OK138555). Genome-sequence annotation revealed G + C and A + T contents of 50.3% and 49.7%, respectively. The genome encodes 80 ORFs that predominantly encode hypothetical proteins with uncharacterized functions. Proteins encoded by the IME328 genome were categorized functionally as structural, regulatory, lytic, or uncharacterized proteins. Notably, integrase genes, virulence factors, and toxin- or antibiotic-resistance genes were not detected in the IME328 genome.

BLAST whole-genome sequence-alignment analysis identified the sequences closest to that of IME328 in the database. The results included the *K. pneumoniae* phages KP1801 (NC:049848.1), mtp3 (NC:047907.1), and vB_KpnS-VAC110 (OM032871.1). Linear alignment of the whole genomes of IME328, KP1801, mtp3, and vB_KpnS-VAC110 revealed a high degree of similarity. This similarity was observed across the entire genome and was particularly pronounced in regions encoding the tail-fiber protein.

3.4. Phylogenetic tree analysis

Genomic comparisons using BLAST analysis demonstrated that the *K. pneumoniae* phage KP1801 (NC:049848.1) shared the highest similarity with IME328, exhibiting 92% homology (NC:049848.1). Phylogenetic tree analysis, focusing on the large terminase subunit, indicated close evolutionary relationships between *vB_KpnM*_IME328 T8 and other *K. pneumoniae* phages, including KP1801, GH-K3, sin41513, and KP36. According to the latest International Committee on Taxonomy of Viruses guidelines (last updated on May 19, 2022)(Grigson et al. 2023), IME328 falls within the *Webervirus* genus of the *Drexlerviridae* family under the *Caudoviricetes* order (Fig. 3A).

3.5. IME328 phage tail-fiber protein phylogenetic analysis

A phylogenetic tree of the IME328 phage tail-fiber protein was constructed using HHpred, with the IME328 phage tail-fiber protein serving as a query. At the protein level, ORF3 of IME328 showed similarity with the active domains of various phage tail-fiber proteins, specifically those associated with polysaccharide hydrolysis. In the phylogenetic tree (Fig. 3B), IME328 and *K. pneumoniae* phage SH-KP2492 exhibited the highest similarity. This similarity suggests a close evolutionary relationship or

shared functional characteristics between tail-fiber proteins. An alignment showed remarkable similarity, with a sequence identity of 99.28% (Fig. 3C).

3.6. Identification of a K62-type depolymerase

Analysis of IME328-ORF3 predicted that it encodes a tail-fiber protein gene that potentially possesses depolymerase activity. Thus, ORF3 was cloned and expressed in the BL21 (DE3) cells. The purified recombinant IME328-ORF3-Dp3 protein was visualized and verified by sodium dodecyl sulfate-polyacrylamide gel electrophoresis (Fig. 4A). When tested on agar plates containing Kp930, the recombinant IME328-ORF3-Dp3 exhibited substantial depolymerase activity.

3.7. Host range and depolymerase activity

The IME328 phage showed a limited lytic spectrum, specifically targeting only the K62-capsule type among *K. pneumoniae* strains with 23 different capsule types (Table 1), with a success rate of 100% (5/5) for the K62 type (Table 1). This specificity aligns with that of a previous study conducted by Wang (Pan et al. 2015).

3.8. Depolymerase activity combined with serum sterilization

To evaluate the sensitizing effect of Dp3 on *K. pneumoniae*, we measured bacterial viabilities under various conditions. Figure 5 shows that the bacterial counts of samples treated with both Dp3 and serum were significantly lower (by over three log decades) than those of samples treated with serum alone ($P < 0.0001$, one-way analysis of variance). Treatment with serum alone did not decrease the bacterial counts. Similarly, treatment with Dp3 alone or in combination with inactivated serum did not affect bacterial survival.

3.9. English Version Synergistic bactericidal activity of Dp3 and serum

To visually confirm the enhanced bactericidal efficacy of Dp3 combined with serum, dual-fluorescence live/dead staining was performed (Fig. 5B). In the control group, the bacteria predominantly exhibited widespread green fluorescence (DMAO) with negligible red signals, indicating high cell viability and intact membrane integrity. In contrast, following co-treatment with Dp3 and serum, the density of green-fluorescent intact cells noticeably decreased, accompanied by a robust accumulation of red fluorescence (PI). The superimposition of the two channels (Merged) in the Dp3 + Serum group revealed a high proportion of yellow/orange signals, which represents membrane-compromised dead bacteria. These imaging outcomes align with the CFU quantification, demonstrating that the depolymerase Dp3 effectively strips the bacterial protective capsule, significantly rendering the bacteria susceptible to serum-mediated killing.

3.10. Dp3 promotes macrophage-mediated bacterial phagocytosis

Capsule depolymerases can expose bacterial surface antigens, thereby facilitating recognition by host immune cells. To confirm this, a phagocytosis assay was conducted using RAW264.7 macrophages and FITC-labeled bacteria (Fig. 5C). In the PBS-treated control group, only sparse green fluorescent signals were observed in the FITC channel, indicating minimal bacterial adherence or engulfment by the macrophages. In contrast, pre-treatment of the bacteria with the depolymerase Dp3 resulted in a dramatic increase in cell-associated green fluorescence. The merged images clearly demonstrate that a large number of FITC-labeled bacteria were tightly adhered to or internalized by the RAW264.7 cells. These morphological observations indicate that the enzymatic degradation of the protective capsule by Dp3 significantly restores and enhances the phagocytic clearance capacity of host macrophages against the bacteria.

3.11. Depolymerase Dp3 significantly improves the survival rate of infected mice

The survival curve demonstrated that following inoculation with a lethal dose of bacteria (6×10^7 CFU), mice in the untreated infection group (Kp930) began to succumb at approximately 15 hours and reached 100% mortality within 32 hours. In stark contrast, all mice treated with Dp3 survived the entire 96-hour observation period (100% survival rate). These results indicate that Dp3 confers complete lethal protection against systemic infection (Figure A).

3.12. Dp3 effectively promotes bacterial clearance in host organs

To investigate the *in vivo* antibacterial capacity of Dp3, we quantified the bacterial load in major organs when the untreated mice were moribund. The bacterial burdens in the liver, spleen, lung, and kidney of the untreated control group were extremely high, reaching approximately 10^6 CFU/g. Conversely, the Dp3-treated group exhibited a dramatic reduction in bacterial loads across all tested organs, dropping to approximately 10^3CFU/g. This indicates that Dp3 profoundly inhibits bacterial dissemination and proliferation within solid organs (Figure B).

3.13. Dp3 alleviates infection-induced histopathological damage

H&E staining revealed intact organ architecture and regular cellular arrangement in the healthy control group. The untreated infected mice (Kp930) exhibited severe pathological changes: the liver showed cellular swelling and inflammatory cell infiltration; the spleen displayed disrupted white pulp and congested red pulp; the lungs presented with thickened alveolar walls, severe hemorrhage, and extensive inflammatory infiltration; and the kidneys exhibited glomerular atrophy and tubular epithelial degeneration. Notably, Dp3 treatment markedly attenuated these pathological lesions, with tissue morphologies largely restored to resemble those of the healthy controls. This demonstrates the efficacy of Dp3 in protecting target organs from infection-mediated structural damage (Figure C).

4. Discussion

The relentless global dissemination of CRKPhas severely compromised our clinical armamentarium, frequently rendering conventional antibiotic regimens ineffective (Leavitt et al. 2021). The primary virulence determinant of this opportunist is its formidable CPS, which establishes a physical barrier that thwarts antimicrobial penetration, neutralizes host complement cascades, and prevents macrophage engulfment(McHardy et al. 2021). While recent surveillance and therapeutic development have largely prioritized highly prevalent serotypes such as K47 and K64, the selective pressure exerted by broad-spectrum antibiotics is driving the emergence of rare, hyper-resistant clones(Huang et al. 2024b; Liu et al. 2020b; Wang et al. 2023). The K62 isolate evaluated in this study (Kp930) exemplifies this emerging threat, exhibiting profound resistance to both broad-spectrum cephalosporins and fluoroquinolones. Given the critical absence of interventions targeting the K62 serotype, this study bridges a significant clinical void by detailing the first isolation and comprehensive characterization of the K62-specific phage, vB_Kp_IME328, alongside its highly potent depolymerase, Dp3.

Genomic and phylogenetic analyses place IME328 within the *Webervirus* genus of the *Siphoviridae* family. Crucially for future translational efforts, the IME328 genome is devoid of known virulence factors, integrated toxins, or antibiotic resistance determinants, fulfilling the strict safety prerequisites for developing phage-derived therapeutics. The most clinically translatable asset of IME328, however, lies in its tail-fiber protein, ORF3. By successfully cloning and expressing this target, we identified Dp3 - an enzyme exhibiting absolute and stringent degradation activity exclusively against K62-type *K. pneumoniae* among 23 diverse capsular types tested. This exquisite specificity offers an immediate diagnostic advantage: Dp3 can be deployed as a rapid, cost-effective, and highly reliable tool for K62 capsule typing, effectively bypassing the logistical and temporal delays associated with traditional *wzc* sequencing.

Beyond diagnostics, the therapeutic promise of Dp3 is anchored in an "anti-virulence" paradigm, which represents a fundamental shift away from the direct bactericidal mechanisms of traditional antibiotics or lytic phages. Antibiotic-induced bacterial lysis frequently triggers massive endotoxin release, exacerbating systemic inflammation(Abedon et al. 2021). In contrast, Dp3 functions as a precision molecular scalpel, selectively stripping the protective CPS layer without lysing the bacterial cell. Our *in vitro* data elucidate the profound immunological consequences of this capsule removal. We demonstrated that pre-treatment with Dp3 rapidly resensitized the highly recalcitrant K62 CRKP strain to serum complement-mediated killing. Furthermore, the enzymatic unmasking of underlying bacterial surface antigens robustly restored immune recognition, dramatically enhancing bacterial adherence and intracellular clearance by host macrophages. By chemically disarming the pathogen, Dp3 effectively strips its immune-evasive phenotype, leaving it entirely vulnerable to the host's innate immune surveillance.

The clinical potential of this innate immune synergy was definitively validated in our lethal murine bacteremia model. Systemic infection with Kp930 (6×10^7 CFU) triggered rapid physiological

deterioration, resulting in 100% mortality in untreated cohorts. Remarkably, a single therapeutic administration of Dp3 completely altered the disease trajectory, conferring absolute (100%) protection and survival. This dramatic rescue is intrinsically linked to the enzyme's capacity to halt systemic dissemination; we observed a multi-logarithmic reduction in bacterial burdens across vital solid organs, which directly correlated with the preservation of tissue architecture and the attenuation of severe infection-induced histopathology.

Collectively, this study not only broadens the repository of characterized phage-derived enzymes but also validates the exceptional dual utility of the novel K62-specific depolymerase Dp3. Given its pinpoint targeting accuracy, minimal collateral disruption to the host microbiome, and fundamentally low propensity to provoke bacterial resistance, Dp3 emerges as a formidable candidate for integration into the next generation of precision antimicrobial frameworks against multidrug-resistant *K. pneumoniae* infections. Future investigations should prioritize evaluating the efficacy of Dp3 in diverse *in vivo* models, such as respiratory infection paradigms, and exploring its potential synergism when formulated into multi-enzyme cocktails to broaden therapeutic coverage against heterogeneous CRKP populations.

5. Conclusion

In summary, Dp3 offers potential benefits for treating, preventing, and controlling severe CRKP infections and for improving the accuracy and efficacy of capsule typing.

Declarations

7. Consent for publication

All authors have read and approved the final version of the manuscript and consent to its publication.

8. Availability of data and materials

The datasets and materials supporting the conclusions of this study are available from the corresponding author upon reasonable request. All essential data are included within the manuscript.

9. Competing interests

The authors declared that there was no conflict of interest.

10. Funding

This work was supported by the Anhui Provincial Natural Science Foundation Youth Project (NO. 2108085QH310), Anhui Provincial Health Research Project (NO. AHWJ2024Aa20650) the Anhui Provincial Translational Medicine Research Fund project (NO. 2023zhyx-C100) and Fuyang Professional and Technical Reserve Talent Project.

11. Author contributions

Can Wang, Lei Zhao, Ruilin Yang and Jinpan Wei characterized its biological characteristics andalso identified IME328. Can Wang performed genome-wide sequencing and genomic analysis. Can Wang and Ruilin Yang drafted the manuscript. Can Wang and Jinpan Wei conceived and designed the experiments. All the authors have read and agreed to the publication of this manuscript.

12. Acknowledgments

The authors thank the Core Facility Center of Anhui Medical University for technical support in phage genome sequencing and bioinformatics analysis. We are grateful to the Experimental Animal Center of The Fifth affiliated Hospital of Anhui Medical University for assistance with animal model construction and ethical compliance.

We acknowledge the Department of Respiratory Medicine at The Fifth and The First affiliated hospital of Anhui Medical University for providing clinical strain resources and laboratory infrastructure. The graphical abstract was created using BioRender.com under an institutional license. Finally, we appreciate the constructive suggestions from three anonymous reviewers during the peer-review process of this manuscript.

References

1. Abedon ST, Danis-Wlodarczyk KM, Wozniak DJ (2021) Phage Cocktail Development for Bacteriophage Therapy: Toward Improving Spectrum of Activity Breadth and Depth. Pharmaceuticals (Basel) 14(10). 10.3390/ph14101019
2. Brenes LR, Laub MT (2025) E. coli prophages encode an arsenal of defense systems to protect against temperate phages. Cell Host Microbe 33(6):1004–1018e5. 10.1016/j.chom.2025.04.021
3. Brunner A, Nemes-Nikodem E, Jeney C, Szabo D, Marschalko M, Karpati S, Ostorhazi E (2016) Emerging azithromycin-resistance among the Neisseria gonorrhoeae strains isolated in Hungary. Ann Clin Microbiol Antimicrob 15(1):53. 10.1186/s12941-016-0166-9
4. Cano V, Moranta D, Llobet-Brossa E, Bengoechea JA, Garmendia J (2009) Klebsiella pneumoniae triggers a cytotoxic effect on airway epithelial cells. BMC Microbiol 9:156. 10.1186/1471-2180-9-156
5. Choi M, Hegerle N, Nkeze J, Sen S, Jamindar S, Nasrin S, Sen S, Permala-Booth J, Sinclair J, Tapia MD, Johnson JK, Mamadou S, Thaden JT, Fowler VG Jr., Aguilar A, Terán E, Decre D, Morel F, Krogfelt KA, Brauner A, Protonotariou E, Christaki E, Shindo Y, Lin YT, Kwa AL, Shakoor S, Singh-Moodley A, Perovic O, Jacobs J, Lunguya O, Simon R, Cross AS, Tennant SM (2020) The Diversity of Lipopolysaccharide (O) and Capsular Polysaccharide (K) Antigens of Invasive Klebsiella pneumoniae in a Multi-Country Collection. Front Microbiol 11:1249. 10.3389/fmicb.2020.01249
6. Ding J, Xu M, Zhang M, Chang J, Hu Z, Yu Y, Yao Y, Shen N, Tai W, Feng L (2026) Epidemiological and functional insights into iroBCDN loss in ST11 carbapenem-resistant hypervirulent Klebsiella pneumoniae. Microbiol Spectr 14(2):e0247925. 10.1128/spectrum.02479-25

7. Dunstan RA, Bamert RS, Belousoff MJ, Short FL, Barlow CK, Pickard DJ, Wilksch JJ, Schittenhelm RB, Strugnell RA, Dougan G, Lithgow T (2021) Mechanistic Insights into the Capsule-Targeting Depolymerase from a Klebsiella pneumoniae Bacteriophage. Microbiol Spectr 9(1):e0102321. 10.1128/spectrum.01023-21
8. Gorodnichev RB, Volozhantsev NV, Krasilnikova VM, Bodoev IN, Kornienko MA, Kuptsov NS, Popova AV, Makarenko GI, Manolov AI, Slukin PV, Bespiatykh DA, Verevkin VV, Denisenko EA, Kulikov EE, Veselovsky VA, Malakhova MV, Dyatlov IA, Ilina EN, Shitikov EA (2021) Novel Klebsiella pneumoniae K23-Specific Bacteriophages From Different Families: Similarity of Depolymerases and Their Therapeutic Potential. Front Microbiol 12:669618. 10.3389/fmicb.2021.669618
9. Grigson SR, Giles SK, Edwards RA, Papudeshi B (2023) Knowing and Naming: Phage Annotation and Nomenclature for Phage Therapy. Clin Infect diseases: official publication Infect Dis Soc Am 77(Supplement5):S352–s359. 10.1093/cid/ciad539
10. Hua Y, Wu Y, Guo M, Ma R, Li Q, Hu Z, Chen H, Zhang X, Li H, Li Q, He P (2022) Characterization and Functional Studies of a Novel Depolymerase Against K19-Type Klebsiella pneumoniae. Front Microbiol 13:878800. 10.3389/fmicb.2022.878800
11. Huang D, Xia R, Chen C, Liao J, Chen L, Wang D, Alvarez PJJ, Yu P (2024a) Adaptive strategies and ecological roles of phages in habitats under physicochemical stress. Trends Microbiol 32(9):902–916. 10.1016/j.tim.2024.02.002
12. Huang T, Zhang Z, Tao X, Shi X, Lin P, Liao D, Ma C, Cai X, Lin W, Jiang X, Luo P, Wu S, Xie Y (2024b) Structural and functional basis of bacteriophage K64-ORF41 depolymerase for capsular polysaccharide degradation of Klebsiella pneumoniae K64. Int J Biol Macromol 265(Pt 2):130917. 10.1016/j.ijbiomac.2024.130917
13. Jaiswal S, Singh DK, Shukla P (2023) Degradation effectiveness of hexachlorohexane (Y-HCH) by bacterial isolate Bacillus cereus SJPS-2, its gene annotation for bioremediation and comparison with Pseudomonas putida KT2440. Environ Pollut 318:120867. 10.1016/j.envpol.2022.120867
14. Khan Mirzaei M, Nilsson AS (2015) Isolation of phages for phage therapy: a comparison of spot tests and efficiency of plating analyses for determination of host range and efficacy. PLoS ONE 10(3):e0118557. 10.1371/journal.pone.0118557
15. Leavitt R, Ash J, Hasenbalg P, Santarelli A, Dietrich T, Schritter S, Wells J, Dawson A, Ashurst J (2021) Real World Utilization of Bamlanivimab at a Rural Community Hospital. Cureus 13(11):e19747. 10.7759/cureus.19747
16. Li J, Sheng Y, Ma R, Xu M, Liu F, Qin R, Zhu M, Zhu X, He P (2021a) Identification of a Depolymerase Specific for K64-Serotype Klebsiella pneumoniae: Potential Applications in Capsular Typing and Treatment. Antibiot (Basel) 10(2). 10.3390/antibiotics10020144
17. Li M, Li P, Chen L, Guo G, Xiao Y, Chen L, Du H, Zhang W (2021b) Identification of a phage-derived depolymerase specific for KL64 capsule of Klebsiella pneumoniae and its anti-biofilm effect. Virus Genes 57(5):434–442. 10.1007/s11262-021-01847-8

18. Liu Y, Leung SSY, Huang Y, Guo Y, Jiang N, Li P, Chen J, Wang R, Bai C, Mi Z, Gao Z (2020a) Identification of Two Depolymerases From Phage IME205 and Their Antivirulent Functions on K47 Capsule of Klebsiella pneumoniae. Front Microbiol 11:218. 10.3389/fmicb.2020.00218
19. Liu Y, Leung SSY, Huang Y, Guo Y, Jiang N, Li P, Chen J, Wang R, Bai C, Mi Z, Gao Z (2020b) Identification of Two Depolymerases From Phage IME205 and Their Antivirulent Functions on K47 Capsule of Klebsiella pneumoniae. Front Microbiol 11:218. 10.3389/fmicb.2020.00218
20. McHardy JA, Selvaganeshapillai V, Khanna P, Whittington AM, Turton J, Gopal Rao G (2021) A case of neck abscess caused by rare hypervirulent Klebsiella pneumoniae, capsular type K20 and sequence type 420. Ann Clin Microbiol Antimicrob 20(1):46. 10.1186/s12941-021-00453-8
21. Mohammadi M, Saffari M, Siadat SD, Hejazi SH, Shayestehpour M, Motallebi M, Eidi M (2023) Isolation, characterization, therapeutic potency, and genomic analysis of a novel bacteriophage vB_KshKPC-M against carbapenemase-producing Klebsiella pneumoniae strains (CRKP) isolated from Ventilator-associated pneumoniae (VAP) infection of COVID-19 patients. Ann Clin Microbiol Antimicrob 22(1):18. 10.1186/s12941-023-00567-1
22. Monteiro R, Pires DP, Costa AR, Azeredo J (2019) Phage Therapy: Going Temperate? Trends Microbiol 27(4):368–378. 10.1016/j.tim.2018.10.008
23. Nang SC, Lu J, Yu HH, Wickremasinghe H, Azad MAK, Han M, Zhao J, Rao G, Bergen PJ, Velkov T, Sherry N, McCarthy DT, Aslam S, Schooley RT, Howden BP, Barr JJ, Zhu Y, Li J (2024) Phage resistance in Klebsiella pneumoniae and bidirectional effects impacting antibiotic susceptibility. Clin Microbiol Infect 30(6):787–794. 10.1016/j.cmi.2024.03.015
24. Pan Y-J, Lin T-L, Chen Y-H, Hsu C-R, Hsieh P-F, Wu M-C, Wang J-T (2013) Capsular types of Klebsiella pneumoniae revisited by wzc sequencing. PLoS ONE 8(12):e80670. 10.1371/journal.pone.0080670
25. Pan Y-J, Lin T-L, Chen Y-Y, Lai P-H, Tsai Y-T, Hsu C-R, Hsieh P-F, Lin Y-T, Wang J-T (2019) Identification of three podoviruses infecting Klebsiella encoding capsule depolymerases that digest specific capsular types. Microb Biotechnol 12(3):472–486. 10.1111/1751-7915.13370
26. Pan Y-J, Lin T-L, Lin Y-T, Su P-A, Chen C-T, Hsieh P-F, Hsu C-R, Chen C-C, Hsieh Y-C, Wang J-T (2015) Identification of capsular types in carbapenem-resistant Klebsiella pneumoniae strains by wzc sequencing and implications for capsule depolymerase treatment. Antimicrob Agents Chemother 59(2):1038–1047. 10.1128/AAC.03560-14
27. Park BH (1956) An enzyme produced by a phage-host cell system. I. The properties of a Klebsiella phage. Virology 2(6):711–718
28. Pertics BZ, Cox A, Nyúl A, Szamek N, Kovács T, Schneider G (2021) Isolation and Characterization of a Novel Lytic Bacteriophage against the K2 Capsule-Expressing Hypervirulent Klebsiella pneumoniae Strain 52145, and Identification of Its Functional Depolymerase. Microorganisms 9(3). 10.3390/microorganisms9030650
29. Squeglia F, Maciejewska B, Łątka A, Ruggiero A, Briers Y, Drulis-Kawa Z, Berisio R (2020) Structural and Functional Studies of a Klebsiella Phage Capsule Depolymerase Tailspike: Mechanistic Insights into Capsular Degradation. Structure 28(6). 10.1016/j.str.2020.04.015

30. V Volozhantsev N, Shpirt M, I Borzilov A, V Komisarova E A, Krasilnikova M, Shashkov VS, V Verevkin V A, Knirel A Y (2020) Characterization and Therapeutic Potential of Bacteriophage-Encoded Polysaccharide Depolymerases with β Galactosidase Activity against Klebsiella pneumoniae K57 Capsular Type. Antibiot (Basel) 9(11). 10.3390/antibiotics9110732
31. Wang C, Li P, Niu W, Yuan X, Liu H, Huang Y, An X, Fan H, Zhangxiang L, Mi L, Zheng J, Liu Y, Tong Y, Mi Z, Bai C (2019) Protective and therapeutic application of the depolymerase derived from a novel KN1 genotype of Klebsiella pneumoniae bacteriophage in mice. Res Microbiol 170(3):156–164. 10.1016/j.resmic.2019.01.003
32. Wang C, Li P, Zhu Y, Huang Y, Gao M, Yuan X, Niu W, Liu H, Fan H, Qin Y, Tong Y, Mi Z, Bai C (2020a) Identification of a Novel Acinetobacter baumannii Phage-Derived Depolymerase and Its Therapeutic Application in Mice. Front Microbiol 11:1407. 10.3389/fmicb.2020.01407
33. Wang C, Li P, Zhu Y, Huang Y, Gao M, Yuan X, Niu W, Liu H, Fan H, Qin Y, Tong Y, Mi Z, Bai C (2020b) Identification of a Novel Acinetobacter baumannii Phage-Derived Depolymerase and Its Therapeutic Application in Mice. Front Microbiol 11:1407. 10.3389/fmicb.2020.01407
34. Wang C, Wang Q, Mi Z, Zhao L, Bai C (2023) Genomic analysis of K47-type Klebsiella pneumoniae phage IME305, a newly isolated member of the genus Teetrevirus. Arch Virol 168(11):280. 10.1007/s00705-023-05900-9
35. Wang G, Zhao G, Chao X, Xie L, Wang H (2020c) The Characteristic of Virulence, Biofilm and Antibiotic Resistance of Klebsiella pneumoniae. Int J Environ Res Public Health 17(17). 10.3390/ijerph17176278
36. Wu J-W, Wang J-T, Lin T-L, Liu Y-Z, Wu L-T, Pan Y-J (2023a) Identification of three capsule depolymerases in a bacteriophage infecting Klebsiella pneumoniae capsular types K7, K20, and K27 and therapeutic application. J Biomed Sci 30(1):31. 10.1186/s12929-023-00928-0
37. Wu JW, Wang JT, Lin TL, Liu YZ, Wu LT, Pan YJ (2023b) Identification of three capsule depolymerases in a bacteriophage infecting Klebsiella pneumoniae capsular types K7, K20, and K27 and therapeutic application. J Biomed Sci 30(1):31. 10.1186/s12929-023-00928-0
38. Wu Y, Wang R, Xu M, Liu Y, Zhu X, Qiu J, Liu Q, He P, Li Q (2019) A Novel Polysaccharide Depolymerase Encoded by the Phage SH-KP152226 Confers Specific Activity Against Multidrug-Resistant Klebsiella pneumoniae via Biofilm Degradation. Front Microbiol 10:2768. 10.3389/fmicb.2019.02768
39. Yan J, Mao J, Xie J (2014) Bacteriophage polysaccharide depolymerases and biomedical applications. BioDrugs 28(3):265–274. 10.1007/s40259-013-0081-y
40. Yin X, Feng Y, Luo H, Fang Q, Yu J, McNally A, Zong Z (2026) Stepwise phage resistance and collateral phage susceptibility in Klebsiella pneumoniae. Emerg microbes infections 2648890. 10.1080/22221751.2026.2648890

Figures

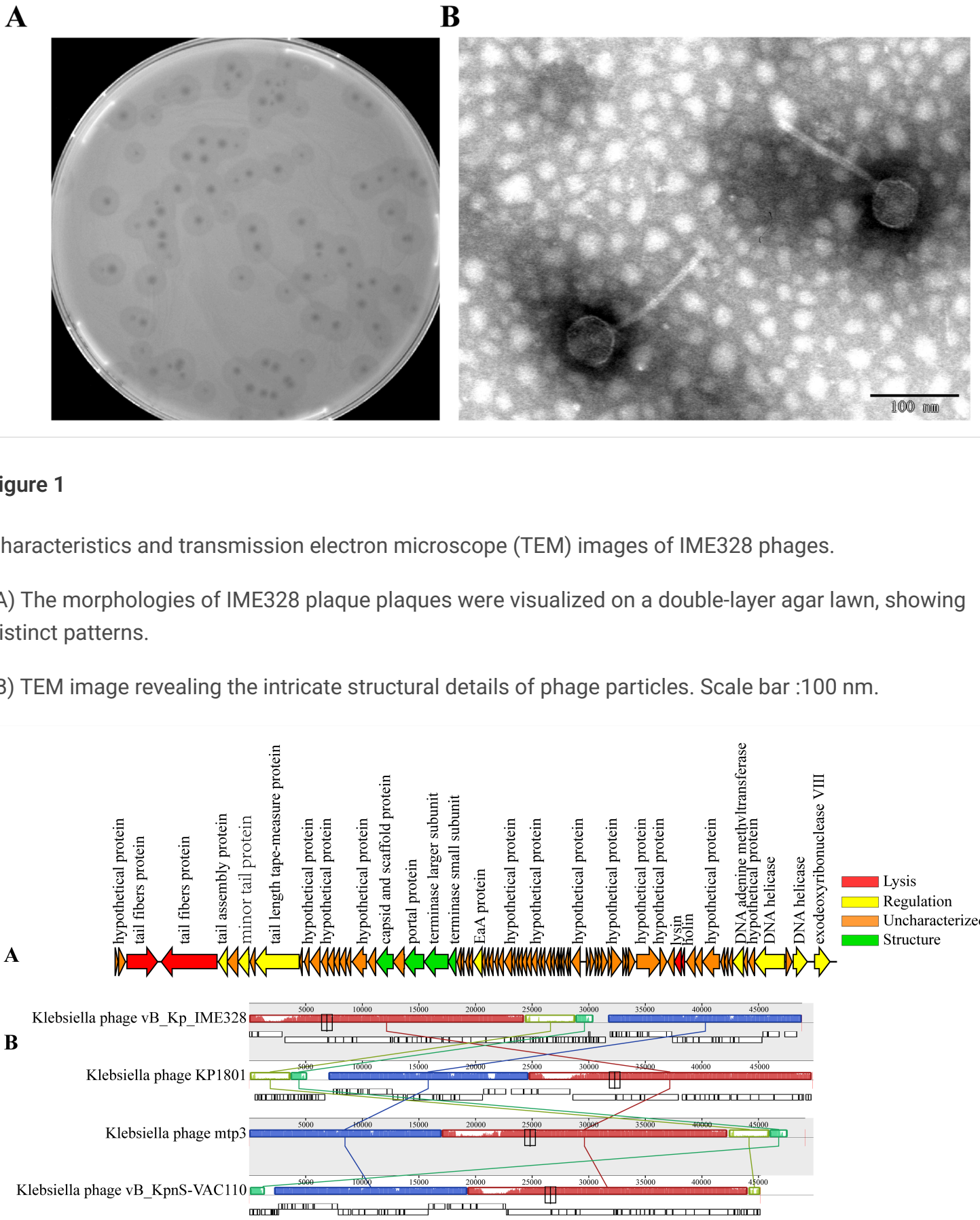


Figure 1

Characteristics and transmission electron microscope (TEM) images of IME328 phages.

(A) The morphologies of IME328 plaque plaques were visualized on a double-layer agar lawn, showing distinct patterns.

(B) TEM image revealing the intricate structural details of phage particles. Scale bar :100 nm.

Figure 2

Linear-genome characteristics of the IME328 phage.

(A) Linear map of the IME328 phage indicating the gene names. The map shows the systematic categorization of all genes into four functional types.

(B) The whole-genome sequence was aligned linearly. Variations in the color intensity represent the sequence homology, with darker hues indicating greater conservation or similarity across genomes.

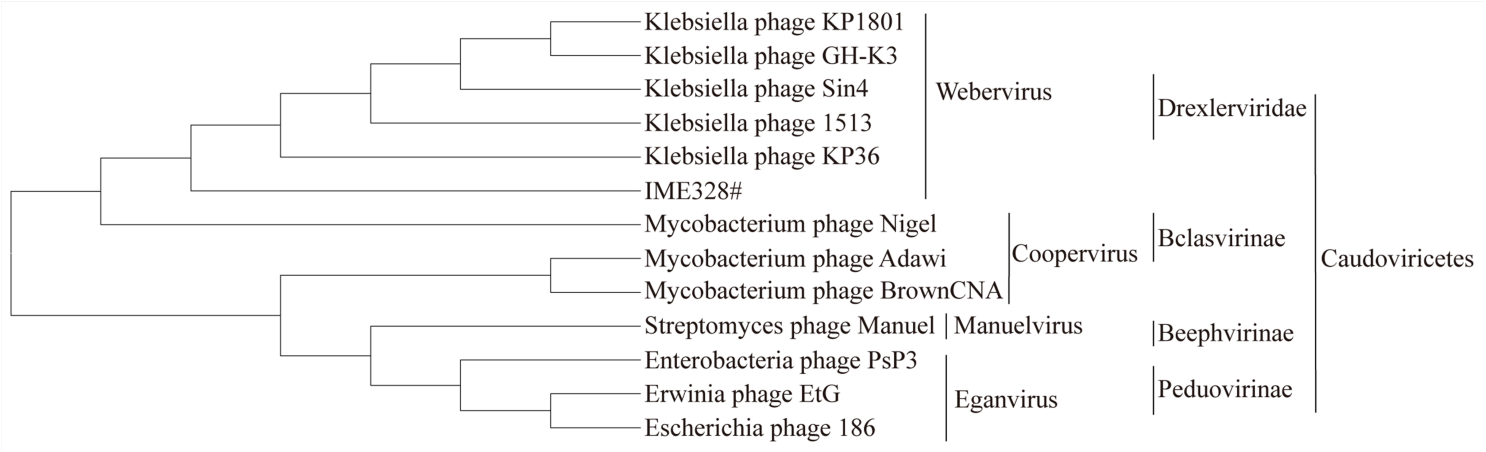


Figure 3

The phylogenetic tree analysis was based on the large subunit of the terminase protein.

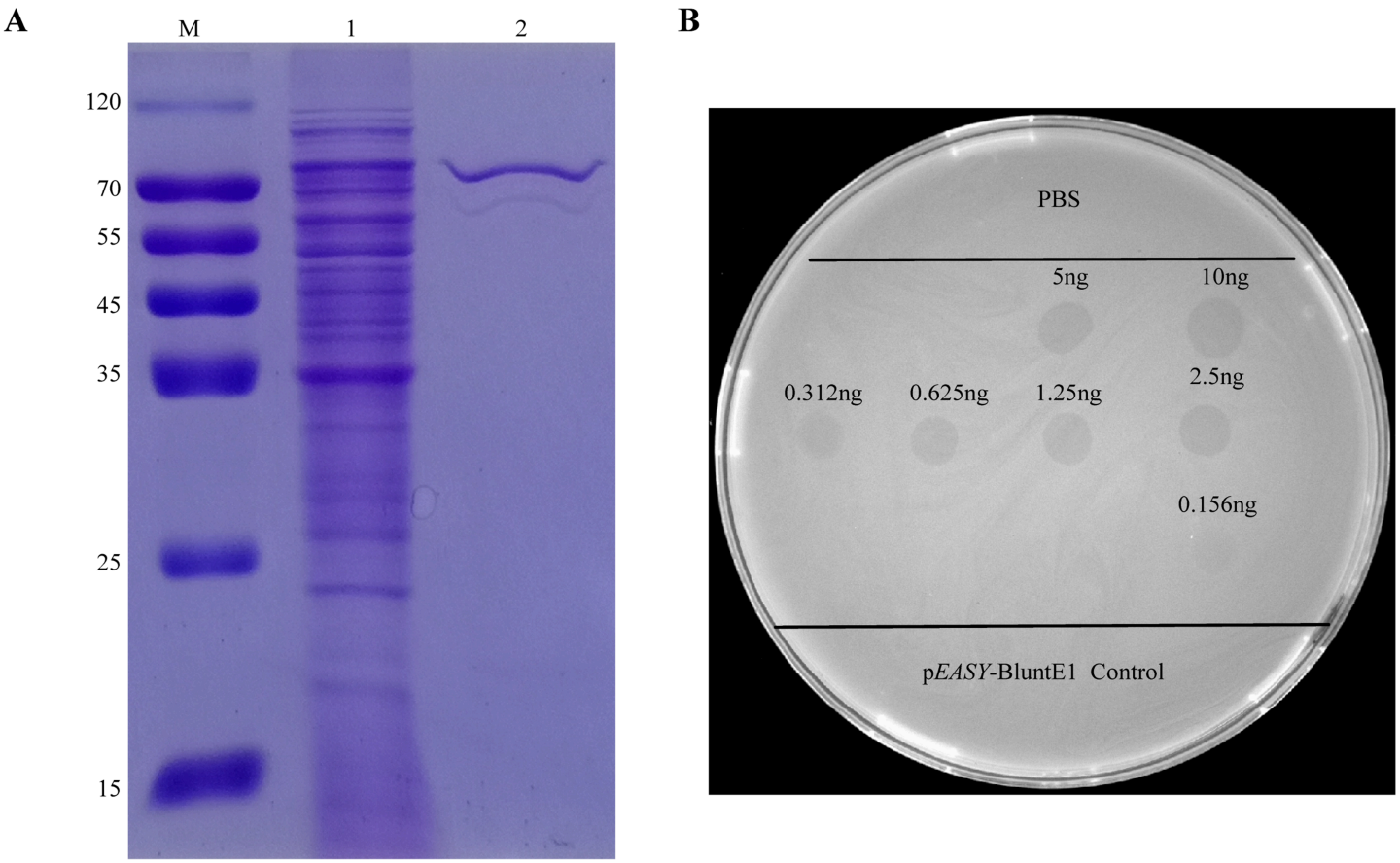


Figure 4

Sodium dodecyl SDS-PAGE analysis of the Dp3 tail-fiber protein and assessment of its depolymerase activity.

(A) SDS-PAGE analysis revealed that the molecular weight of Dp3 was approximately 76 kDa. Lane M represents the molecular-weight marker. Lane 1 shows the total protein extract, which represents the overall protein profile of the sample. Lane 2 highlights purified Dp3 post-affinity chromatography using a nickel (Ni^{2+}) nitrilotriacetic acid column.

(B) The depolymerase activity of Dp3 was evaluated at seven different concentrations, with reference to PBS negative-control group.

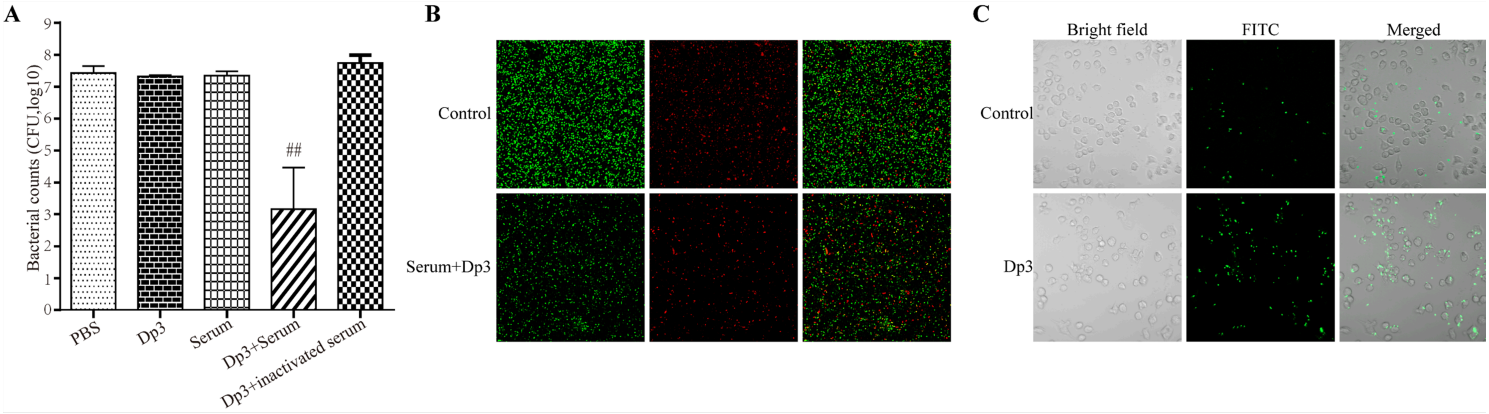


Figure 5

Synergistic antibacterial activity and cellular interactions mediated by depolymerase Dp3.

(A) Efficacy of the Dp3 depolymerase in enhancing serum sterilization. Sensitivity experiments demonstrated that adding Dp3 resulted in higher serum sterilization than observed with the Dp group, the serum-only group, and the group treated with both inactivated serum and Dp. ## $P < 0.001$, versus the DP, serum-only, and Dp + inactivated serum groups.

(B) Representative fluorescence microscopy images of LIVE/DEAD bacterial staining. Bacteria were treated with PBS (Control) or a combination of active serum and Dp3. Green fluorescence (DMAO) indicates viable bacteria with intact cell membranes, whereas red fluorescence (PI) indicates dead bacteria with compromised membranes.

(C) Fluorescence microscopy evaluation of bacterial interaction with host cells. FITC-labeled bacteria (green) were co-incubated with cultured cells after treatment with or without Dp3 (Control). Bright-field, FITC channel, and merged images demonstrate that Dp3 treatment remarkably enhanced the adherence/phagocytosis of bacteria by the cells.

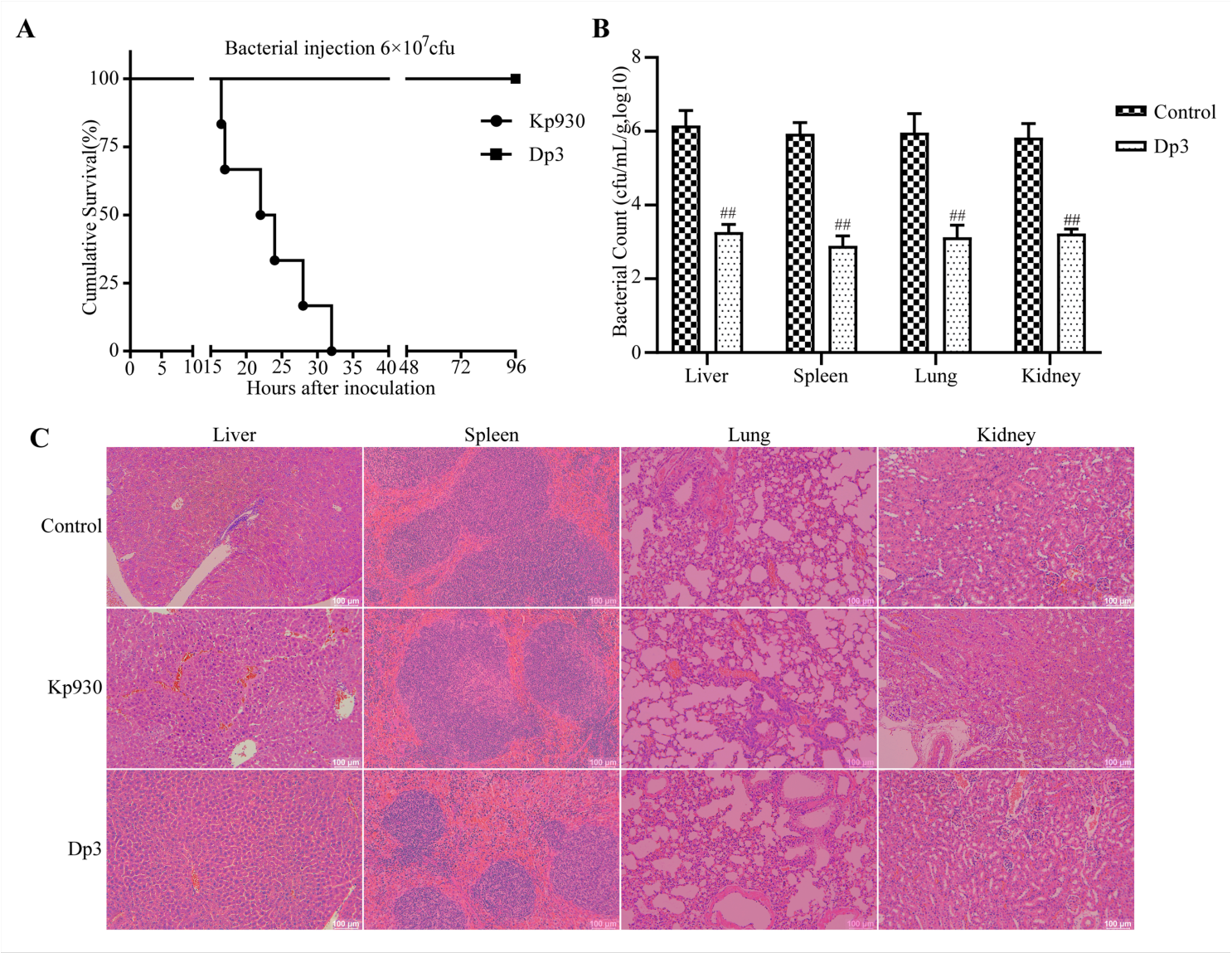


Figure 6

***In vivo* therapeutic efficacy and tissue protection of depolymerase Dp3.**

(A) Kaplan-Meier survival curves. Mice were challenged with 6× 10^7 CFU of bacteria, and the survival rates of the untreated (Kp702) and treated (Dp3) groups were recorded over 96 hours. (B) Bacterial loads in target organs. Liver, spleen, lung, and kidney tissues were harvested during the moribund stage of the untreated mice to quantify bacterial burden (expressed as Log10 CFU/g). Data are presented as mean ± SD; ## indicates statistical significance compared to the untreated Control group.

(C) Representative H&E staining images of the liver, spleen, lung, and kidney (Scale bar = 100 μm). 'Control' represents the healthy mice, 'Kp930' represents the untreated infected mice, and 'Dp3' represents the depolymerase-treated mice.